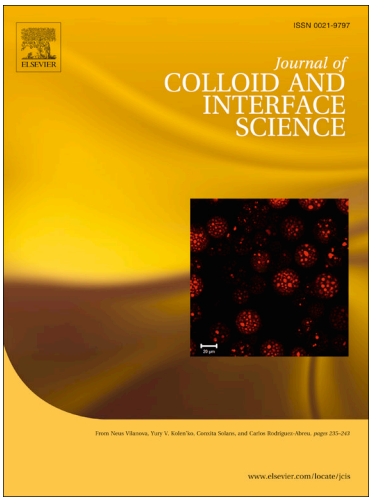

Self-assembled nanofibrils from RGD-functionalized cellulose nanocrystals to improve the performance of PEI/DNA polyplexes

Sry D. Hujaya, Aki Manninen, Kirsten Kling, Jakob B. Wagner, Seppo J. Vainio, Henrikki Liimatainen

PII: S0021-9797(19)30674-5
DOI: https://doi.org/10.1016/j.jcis.2019.06.001
Reference: YJCIS 25039

To appear in: *Journal of Colloid and Interface Science*

Received Date: 5 April 2019
Revised Date: 31 May 2019
Accepted Date: 2 June 2019

Please cite this article as: S.D. Hujaya, A. Manninen, K. Kling, J.B. Wagner, S.J. Vainio, H. Liimatainen, Self-assembled nanofibrils from RGD-functionalized cellulose nanocrystals to improve the performance of PEI/DNA polyplexes, *Journal of Colloid and Interface Science* (2019), doi: https://doi.org/10.1016/j.jcis.2019.06.001

Self-assembled nanofibrils from RGD-functionalized cellulose nanocrystals to improve the performance of PEI/DNA polyplexes

Sry D. Hujaya,[a] Aki Manninen,[b] Kirsten Kling,[c] Jakob B. Wagner,[c] Seppo J. Vainio,[d] Henrikki Liimatainen,[a]*

[a] Fibre and Particle Engineering Research Unit, University of Oulu, P. O. Box 4300, FI-90014 Oulu, Finland. *) Corresponding author. E-mail address: Henrikki.Liimatainen@oulu.fi.

[b] Center for Cell-Matrix Research, Biocenter Oulu, University of Oulu, P. O. Box 5000, FI-90014, Finland.

[c] National Research Centre for the Working Environment, Technical University of Denmark, Lersø Parkallé 105, Copenhagen DK-2100, Denmark.

[d] Laboratory of Developmental Biology, Biocenter Oulu, University of Oulu, P. O. Box 5000, FI-90014 Oulu, Finland.

Abstract

Cellulose nanocrystals (CNCs) are promising bio-derived nanomaterials for the bottom-up fabrication of biomedical constructs. In this report,

dicarboxylic acid-functionalized CNC (DCC) was functionalized with arginylglycylaspartic acid (RGD) tripeptide as a motif for improved cell adhesion and targeting. The product (DCC-RGD) self-assembled into a more elongated nanofibrillar structure through lateral and end-to-end association. When added into poly(ethylene imine) (PEI)/pDNA polyplex solution, nanocelluloses interacted electrostatically with positively charged polyplexes without affecting their integrity. The constructs were tested for their potentials as non-viral transfection reagents. Cell viability and transfection efficiency of fibroblast NIH3T3 cells were monitored as a function of CNC concentration where, in general, viability increased as the CNC concentration increased, and transfection efficiency could be optimized. Using wild-type MDCK and αV-knockout MDCK cells, the construct was able to provide targeted uptake of polyplexes. The findings have potential applications, for example, cell-selective *in vitro* or *ex vivo* transfection of autologous mesenchymal stem cells for cell therapy, or bottom-up design of future innovative biomaterials.

KEYWORDS: cellulose nanocrystals; gene therapy; RGD; targeting; transfection; poly(ethylene imine)

ABBREVIATIONS

PEI, poly(ethylene imine); CNC, cellulose nanocrystal; DCC, dicarboxylic acid-functionalized CNC; RGD, Arginylglycylaspartic acid; MDCK, Madin-Darby canine kidney cells; WT, wild type; MDCK-αVKO, αV-knockout MDCK; MDCK-WT, wild type MDCK; EDC, 1-ethyl-3-(3-dimethylaminopropyl)carbodiimide; NHS, N-hydroxysuccinimide; HEPES, 2-[4-(2-Hydroxyethyl)-1-piperazinyl]ethanesulfonic acid; HBG, HEPES buffered glucose; DAC, dialdehyde cellulose; DMEM, Dulbecco's modified eagle medium; MEM, minimum essential medium; N/P, nitrogen to phosphate; DNA, deoxyribonucleic acid; pDNA, plasmid DNA; PP, PEI/pDNA polyplex; SEM, scanning electron microscopy; cryo-SEM, cryo-scanning electron microscopy; DLS, dynamic light scattering; TE, transfection efficiency; FACS, fluorescence-activated cell sorting; -Ctrl, non-treated control; PDI, polydispersity index.

1. Introduction

Nanocelluloses are emerging nanomaterials derived from renewable natural sources. They have opened doors for new applications in various fields, particularly due to their exceptional properties, including their high mechanical strength, biocompatibility and limited toxicity. Cellulose nanocrystals (CNCs) are typically defined as the smallest crystalline unit of hierarchically structured, hydrogen-bonded cellulose chains. CNCs differ in dimension depending on their natural source but are generally rod-shaped with a high aspect ratio. Their width ranges from 2–50 nm, while their length may range from 100–2000 nm [1].

CNCs have been used as nanoadditives in various composite structures, from catalysis [2] and packaging materials with advanced barrier properties [3, 4] to biomedical applications, such as antibacterial nanomaterial [5], enzyme activity preservation [6], bioimaging [7-9] cellular targeting [10, 11], virus extraction [12], and as a gene delivery vector [13, 14]. CNCs are also attractive as natural building blocks for designing bottom-up approaches to fabricate three-dimensional nano-structured entities especially due to their tailorable chemical characteristics. The formation of ordered 3D nanostructures from CNCs,

for example, through complementary DNA hybridization [15] and directed crosslinking [16], has been reported to result in mushroom-like shapes [17] and nanoplatelet gels [18].

Here, we report the formation of self-assembled nanofibrils from RGD-functionalized CNCs (DCC-RGD). First, dicarboxylic acid-functionalized CNC (DCC) were synthesized using sequential oxidation with periodate and chlorite, respectively, followed by the functionalization of the carboxylic acid groups with RGD tripeptide through EDC/NHS coupling. During the synthesis, the individual CNCs spontaneously self-assembled into nanofibrillar structures (Figure 1). We chose RGD as a recognition motif as it is known to promote cell adhesion. Moreover, a receptor for the RGD motif includes, among others, αVβ3 integrin which is also known to be overexpressed in certain cancers [19], making it a popular motif for targeted gene therapy [20] and biomaterial surface engineering [21, 22].

In this report, we investigated the potential of the self-assembled RGD-functionalized nanofibrillar structure to improve transfection efficiency of PEI/pDNA polyplexes (PP) *in vitro* in comparison with the colloidal

CNC (i.e., DCC). PEI/pDNA polyplex is a widely used gene delivery system that is prepared by mixing poly(ethylene imine) (PEI) and DNA at a known nitrogen to phosphate (N/P) ratio. The mixture can spontaneously form spherical constructs with a diameter in the range of 50–200 nm. PEI is known to effectively facilitate the cellular uptake as well as intracellular release of the DNA cargo; however, it is also indicated to be cytotoxic, particularly at a higher N/P ratio [23, 24].

We propose that both self-assembled nanofibrillar RGD-functionalized CNCs and colloidal DCC CNCs may interact through electrostatic interactions with pre-formed PP and may further act as an additional coating or matrix that reduce the polyplexes' surface charges. This, in turn, can reduce cytotoxicity associated with PP. We also expect that the proposed constructs may alter cellular recognition due to the elongated shapes of both DCC CNCs and the self-assembled nanofibrillar RGD-functionalized CNCs, with respect to spherical shapes, as reported previously [10, 25, 26]. Finally, we monitored these constructs for their ability to induce preferential uptake on wild type-MDCK (MDCK-WT) against αV-integrin knockout-MDCK (MDCK-αVKO) cell lines. The

results in this report demonstrate the potential of CNCs as functionalizable nano-sized building blocks for biomedical applications.

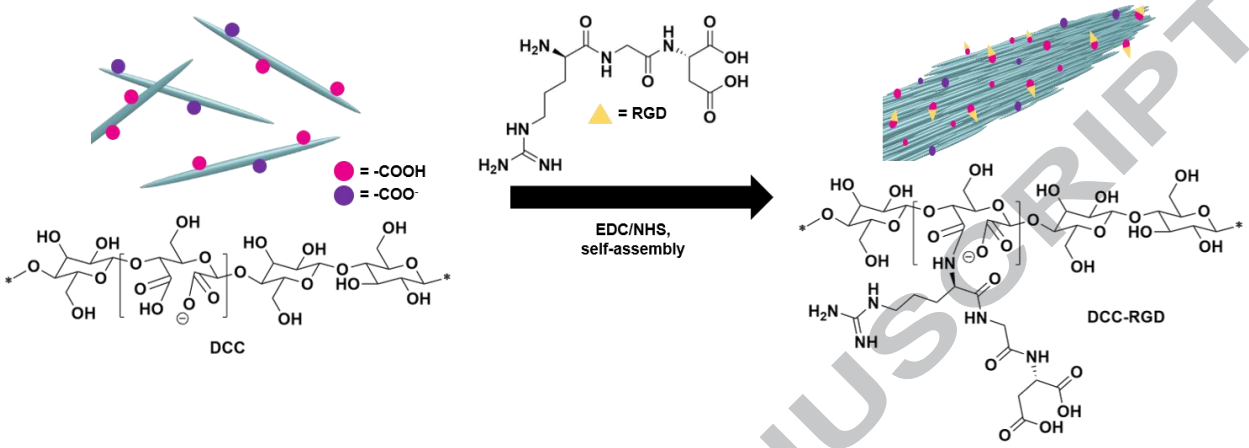

Figure 1. Schematic representation of DCC, its functionalization with RGD tripeptide and self-assembly into DCC-RGD. At the physiological pH, carboxylic acid groups are partially ionized, giving the particles partial negative charges on their surface that may interact with positively charged structures such as the polyplexes.

2. Materials and Methods

Sodium periodate ($NaIO_4$, ≥99.8%, Sigma-Aldrich), sodium chlorite ($NaClO_2$, 80%, Sigma-Aldrich), acetic acid (CH_3COOH, glacial, 100%, Merck), Arg-Gly-Asp tripeptide (RGD, ≥97%, Sigma-Aldrich), 1-ethyl-3-(3-dimethylaminopropyl)carbodiimide (EDC, ≥98%, TCI), 2-[4-(2-Hydroxyethyl)-1-piperazinyl]ethanesulfonic acid (HEPES, >99%, TCI), *N*-hydroxysuccinimide (NHS, 98%, Sigma-Aldrich), linear poly(ethylene imine) average MW 25 000 (PEI, ≥95%, Polysciences), and pCMV-GFP (pDNA, PlasmidFactory) were purchased and used

without further purification. Commercial bleached birch kraft pulp was used as the cellulose raw material. HEPES buffered glucose (HBG) buffer solution was prepared by dissolving HEPES at 20 mM and glucose at 5 wt% in deionized water and adjusting the pH to 7.4.

2.1. Conductometric Titration

Conductometric titration was performed on an Excellence Titrator T5 (Mettler Toledo, USA) according to the method described in the literature [27].

2.2. Elemental Analysis

The nitrogen content in RGD-functionalized CNC was measured using an elemental analyzer (PerkinElmer 2400 Series II CHNS/O Analyzer, USA). Samples were dried via freeze drying and kept in a desiccator until measurements were performed.

2.3. Preparation of Dicarboxylic Acid Cellulose Nanocrystals (DCC)

DCC was prepared by first immersing 15 g of bleached birch pulp in 1.5 L of deionized water overnight, followed by mechanical disintegration. The suspension was then brought to 65 °C in a water bath and reacted with sodium periodate (12.3 g) in the presence of LiCl (27 g) for 3 h in the dark. The suspension was then filtered through 12–15

μm filter paper and washed with deionized water. The resulting dialdehyde cellulose (DAC) was then collected and stored at 4 °C in the non-dried state.

DCC was synthesized by reacting DAC (6 g dry weight) with 5.24 g of sodium chlorite and 6.12 g of 30% sodium peroxide in 1 M acetic acid solution in deionized water for 2 days at room temperature. After the reaction, the product was filtered through 12–15 μm filter paper, washed with deionized water, and sampled to measure the dry matter content. The remaining product was suspended into a 0.5 % w/w concentration in deionized water and passed through a double-chamber system (400 and 200 μm) at a pressure of 1000 bar in a microfluidizer (Microfluidics M-110EH-30 microfluidizer, USA). The final DCC CNC suspension was obtained at a concentration of 5.6 mg/mL in deionized water and used as such in the wet state. The DCC suspension for cell transfection studies was autoclaved and stored frozen for preservation.

2.4. Preparation of RGD-Functionalized DCC (DCC-RGD)

The RGD functionalization of DCC was carried out by first activating 20.0 mL of DCC suspension with 75.3 mg of EDC at room temperature (RT) and maintaining a pH of ~4 by the addition of HCl (0.5 M). After

10 min, 33.2 mg of NHS was added into the suspension, and the reaction was left to proceed for 30 min at RT. The pH of the solution was then increased to ~8 with NaOH (0.5 M), followed by the addition of 50 mg of RGD. The reaction continued for 4 h at RT while the pH was maintained at ~8. Afterwards, the dispersion was purified from excess reactants and salts via dialysis in a dialysis tubing with a 14,000 Da molecular weight cut-off (Sigma-Aldrich) for 3 days. The purified dispersion was then autoclaved for sterilization and stored frozen for preservation. The concentration was determined through gravimetric analysis to be 2.87 mg/mL Briefly, a known volume of the dispersion was freeze-dried and weighed in triplicate to obtain the concentration of the CNCs in the dispersion.

2.5. Preparation of PEI/pDNA Polyplex (PP)

To minimize the effect of variability of polyplex composition, the results reported in this study were obtained with a constant polyplex formulation. Notably, N/P ratio and presence/absence of serum in the formulation were previously investigated on NIH3T3 cell line, and the following reported formulation was found to be optimal (Figure S1).

PP was prepared by adding PEI solution to 75 μg/mL pDNA solution at 4/1 v/v ratio in HBG pH 7.4. The mixture was vortexed for 5 seconds and incubated at RT for 30 min. The concentration of PEI was adjusted to a 10/1 N/P ratio, i.e., the ratio of amine groups on PEI to the phosphate groups on pDNA.

2.6. Addition of CNC to PEI/pDNA Polyplex

A frozen stock of CNC dispersions was left to thaw at RT and rigorously vortexed before use. The concentration was adjusted by diluting from the stock dispersion with an appropriate amount of HBG. CNC was added at the end of the polyplex's 30–min incubation at a 10% volume of the polyplex, followed by an additional 10 min of incubation at RT. Moreover, the concentration of the added CNC dispersion was varied to study its effects. The highest concentration of CNC dispersion added into PP solution was 2 mg/mL which corresponds to a final concentration of 182 μg/mL. For simplicity, PP/CNC constructs are labeled as **PP/CNCX** with ***CNC*** referring to the type of CNC (i.e., either DCC or DCC-RGD) and ***X*** representing the concentration of the added CNC dispersion in mg/mL. For example, PP/DCC-RGD2 represents PP

added with 2 mg/mL of DCC-RGD at 1/10 the volume of the polyplex (i.e., the final concentration of DCC-RGD in the mixture is 182 μg/mL). The PP solution is always prepared the same way as described in Section 2.5, unless otherwise noted.

To study of the effect of sonication on transfection efficiency and viability, a 2 mg/mL dispersion of DCC-RGD in HBG was sonicated on ice with a Q800R sonicator (QSonica, USA) at 50% amplitude, 30 s on/30 s off cycle for 5 min. The dispersion was then added into a prepared polyplex solution and used as previously described.

2.7. Gel Retardation Assay

The samples for gel retardation assay were prepared by mixing 17.6 μL of polyplex or polyplex/CNC complex in HBG with 3 μL of loading buffer. From the mixture, 15 μL sample was loaded into a 1.5 wt% agarose gel containing Midori Green, and electrophoresed for 80 min at 80V in TAE running buffer. Pictures of the gel were then taken and optimized on a Gel Doc™ XR+.

2.8. Cryo-Scanning Electron Microscopy (Cryo-SEM)

Cryo-scanning electron microscopy (Quanta 200 FEG ESEM, equipped with Quorum cryo transfer system and stage) was used to

illustrate the morphology of aqueous PP in the presence and absence of DCC2 and RGD-DCC2. The specimens prepared in water as described above (Sections 2.5 and 2.6) were dipped into slushed liquid N_2, were inserted into and fractured in the preparation chamber at high vacuum and then transferred to the SEM chamber (-190 °C) for pre-imaging. After 1 h of sublimation (-70 °C) in the SEM chamber, the sample was retracted into the preparation chamber and coated (6 seconds) with Pt, before it was transferred back to the SEM chamber for imaging (-90 °C) at 12 kV.

2.9. Dynamic Light Scattering (DLS)

All polyplex samples were prepared in HBG buffer as previously described. CNCs were also characterized in the absence of polyplex by preparing them in HBG at a 1 mg/mL concentration. The z-average and ζ-potential were measured on a Zetasizer Nano ZS (Malvern Instruments, UK). Samples were equilibrated for 120 seconds in the instrument before starting the measurements. Measurements were carried out at 25 ± 0.1 °C and each sample was measured three times. The Z-average (cumulant method) results from the Zetasizer software

were reported as sizes with dispersant refractive index at 1.330 and the viscosity of 0.8872 cP.

2.10. Cell Culture

NIH3T3 cells were grown in Dulbecco's modified eagle medium (DMEM) containing 4.5 g/L glucose and GlutaMAX™ (Gibco) supplemented with 1% (v/v) PennStrepp (Sigma-Aldrich) and 10% (v/v) fetal bovine serum (Gibco). Cells were cultured at 37 °C in a 5% CO_2 incubator, trypsinized at about 90% confluency, and split at a 1:5 or 1:6 ratio.

Wild–type MDCK (MDCK-WT) and αVKO MDCK (MDCK-αVKO) were grown in a minimum essential medium (MEM) containing GlutaMAX™ (Gibco) supplemented with 1% (v/v) PennStrepp (Sigma-Aldrich) and 5% (v/v) fetal bovine serum (Gibco). Cells were cultured at 37 °C in a 5% CO_2 incubator, trypsinized at about 90% confluency, and split at 1:5 or 1:10 ratio.

2.11. Lentivirus-mediated Gene Knockout

Gene editing with Cas9 and sgRNA expressing lentivirus (LentiCRISPR) was achieved as previously described [28]. A target sequence CCTGCGCCCCGCTGTACCAC, with no off-target sites with

less than three mismatches in the *canis lupus familiaris* genome, was selected from exon 3 of the dog integrin αV gene. gRNA oligos with BsmBI (New England Biolabs) overhangs (Oligo1: CACCG CCT GCG CCC CGC TGT ACC AC; Oligo2: AAAC GTG GTA CAG CGG GGC GCA GGC) were subcloned into lentiCRISPR v2 (a gift from Dr. Feng Zhang, Addgene plasmid # 52961) and used for lentivirus preparation. To produce lentiviruses, 70-80% confluent 293T-D10 on CellBind® 10 cm Ø tissue culture dishes (Corning) were co-transfected with the CRISPR-construct, psPAX2 (a gift from Dr. Didier Trono, Addgene plasmid # 12260) and VSVg (a gift from Didier Trono, Addgene plasmid # 12259) plasmids using Lipofectamine® 2000 reagent (Thermo Fisher Scientific) in Opti-MEM™ (Thermo Fisher Scientific). For infection, viral supernatant was used as described before [29]. Subconfluent MDCK cells, seeded at a density of 6 x 10^4/24-well the previous day, were infected for a period of 24 h, expanded for another 24 h without virus and then trypsinized, reseeded and cultured for 24 h in the presence of 4 µg/ml puromycin to select transduced cells. Clonal

cell lines were established from the puromycin resistant population and analyzed by western immunoblotting for loss of αV-integrin expression.

2.12. Cell Transfection

Cells were counted (TC20 Automated Cell Counter, Bio-Rad, USA) and seeded in a 96-well plate at a density of 8,000 cells/well (NIH3T3) or 18,000 cells/well (MDCK-WT and MDCK-αVKO). After 24 h, the medium was removed, and cells were washed once with 200 µL of PBS. Then, 100 µL of fresh medium was added to each well, followed by 100 µL of the polyplex solution. Cells were then incubated for 4 or 48 h. After the incubation, the conditioned medium was removed, cells were washed and added with fresh complete medium. The cells were then further cultured for 2 days.

2.13. Cytotoxicity of CNCs

NIH3T3 cells were seeded in a 96-well plate at a density of 8,000 cells/well. After 24 h, the medium was removed, and cells were washed once with 200 µL of PBS. Then, 200 µL of medium containing CNC at various concentrations was added to each well. Cells were then incubated for another 48 h. Both during seeding, culture, and treatment of the cells, complete DMEM medium containing serum as indicated in

Section 2.10 was used. CNCs were diluted in this complete medium to the desired concentration and subsequently transferred on wells containing the cell monolayer.

2.14. Metabolic Activity Assay Post-transfection

Two days after the introduction of transfection construct or CNC at various concentrations, 10X AlamarBlue was added to each well at 10% v/v and incubated for 4–6 h. The fluorescence intensity of resorufin (i.e., metabolically-reduced resazurin) was then recorded using a Victor^3 plate reader (PerkinElmer, USA). Cells grown in complete DMEM without constructs or CNC were regarded as positive controls. All fluorescence intensities recorded were corrected by subtracting the values with those of no-cell control wells. All cell experiments were carried out in triplicates.

2.15. Fluorescence Microscopy

For fluorescence imaging, two days after the introduction of transfection construct or CNC, conditioned media were removed, cells were washed with DPBS, stained with Hoechst 33342 and propidium iodide, and imaged under a cellSense fluorescence microscope

(Olympus, Japan). Images were further processed using ImageJ/FIJI (National Institute of Health, MD) [30].

2.16. Quantification of Transfection Efficiency (TE) by Flow Cytometry

Forty-eight hours after transfection, conditioned media were removed and cells were washed once with complete fresh media, supplemented with 100 µL of 0.25% trypsin, incubated for 5 min at 37 °C and then kept on ice until flow cytometry measurements (FACSCalibur, Becton-Dickinson). Expressed GFP was excited at 488 nm and emission was detected via a 530 nm band-pass filter. Experiments were done in triplicates and a minimum of 10 000 events were measured for each replicate. Data analysis was performed using the FACS Cellquest Software. A Dot plot was applied to separate the live cell population from dead cells and debris, and a marker was used to quantify the transfection efficiency within this live cell population. The same gate and marker settings were used for all experiments with the same cell line.

2.17. Statistical Analysis

Cell culture experiments were performed independently at least twice to check for reproducibility. The viability and transfection efficiency data were from one experiment with at least three replicates. Data were analyzed and plotted with the GraphPad Prism version 6.01 software. All data represent means ± standard deviation. Statistical significance analysis was performed based on the two-sample t-test and the difference was significant when $p < 0.05$.

3. Results and Discussion

3.1. Syntheses of DCC and DCC-RGD

DCC nanocrystals were obtained as a stable water-like suspension and stored in never-dried state at 4 °C. The concentration was calculated through gravimetric analysis to be 5.6 mg/mL. Throughout the study, neither flocculation nor aggregation was observed. The high stability stemmed from the high concentration of carboxylic acid group. Based on conductometric titration, we found carboxylic acid concentration of 1.85 mmol/g of dry DCC.

The functionalization of carboxylic acid groups of DCC nanocrystals with RGD tripeptide was performed via carbodiimide coupling (Figure 1). The degree of functionalization was estimated through elemental analysis to be 0.12 mmol RGD/g of dry content.

The formation of an elongated, fibrillar structure from individual nanocrystals was noticeable during the coupling reaction and subsequent dialysis as translucent flocculant. To preserve the self-assembled structure, the product was stored frozen in its never-dried dispersion state after dialysis and autoclaving. To calculate the concentration, gravimetric analysis was performed on a portion of the dispersion. The final dispersion concentration was 2.87 mg/mL.

3.2. Cytotoxicity of DCC and DCC-RGD

To investigate the biocompatibility of the prepared DCC and DCC-RGD, both CNCs were incubated with NIH3T3 cells at the specific range of concentrations used throughout this study for 48 h. Biocompatibility was quantified by the extent of cells' metabolic activity in comparison to the non-treated controls (-Ctrl) through the AlamarBlue assay. In this assay, resazurin is metabolically reduced into resorufin

($\lambda_{ex}/\lambda_{em}$ = 545/590 nm), and the amount of resorufin is an indication of the overall metabolic activity of the cell population.

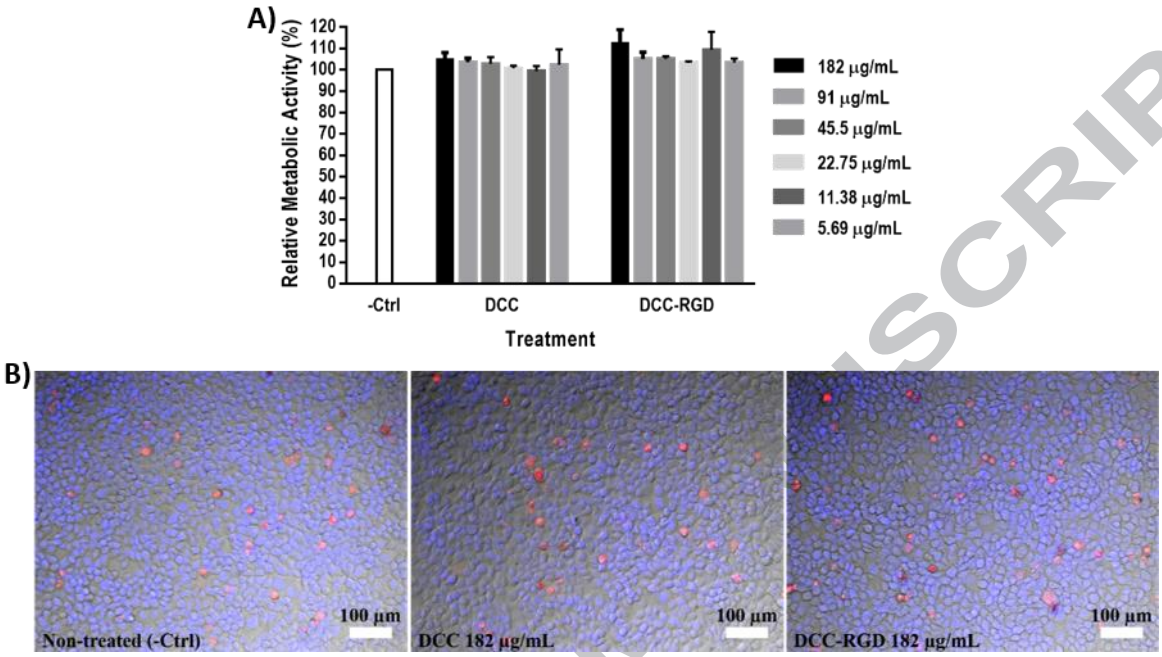

Figure 2. (A) Metabolic activity of NIH3T3 cells after 48–h incubation with either DCC or DCC-RGD at various concentrations, relative to the activity of non-treated cells (-Ctrl). (B) Overlay fluorescence microscopy images of NIH3T3 cells at the end of 48 h of treatment with or without CNCs. CNC treatment was conducted at a concentration of 182 µg/mL. Live cells were stained for their nuclei with Hoechst 33342 (blue), and dead cells were stained with propidium iodide (red).

Figure 2 shows the relative metabolic activity of NIH3T3 cells following 2 days of treatment with various concentrations of DCC or DCC-RGD. At the maximum concentration of 182 µg/mL studied, both DCC and DCC-RGD did not cause any cytotoxic effect and metabolic

activity was maintained at a comparable level to the non-treated control group.

3.3. Polyplex (PP)/CNC Formulation and Gel Retardation Assay

A gel retardation assay was performed to investigate whether the addition of CNC may disrupt polyplex integrity, which, in turn, may lead to the premature release of pDNA. In this assay, constructs were loaded into midori green-containing agarose gel and run for 80 min, after which a photograph of the gel was recorded.

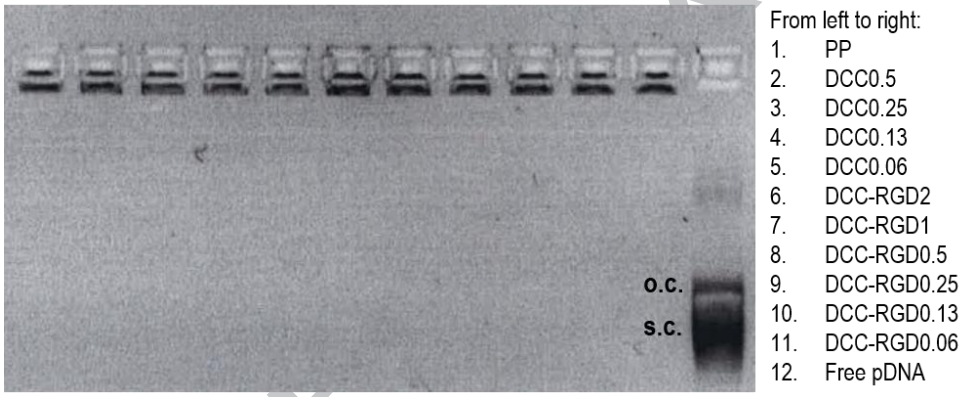

Figure 3. Gel retardation profiles of various polyplex constructs without (lane 1) and with various concentrations of added CNCs (lane 2-11) and compared with free uncomplexed pDNA (lane 12).

The addition of CNCs at various concentrations did not lead to the destabilization of PP (Figure 3). Thus, pDNA remained complexed and could not electrophorese. Only the lane containing free pDNA showed migration of pDNA band. The pDNA was mainly found in a supercoiled

conformation with a small portion found in an open circular conformation. Moreover, constructs displayed relatively weaker fluorescence intensity than the bands from free pDNA due to the pDNA being complexed by PEI.

3.4. Cryo-Scanning Electron Microscopy Imaging (Cryo-SEM)

As opposed to polyplexes that are spherical, CNCs have high aspect ratios. Consequently, a more direct and accurate way of observing the shape of a polyplex/CNC composite is through a microscopy technique instead of indirect light scattering methods. To this end, we performed cryo-SEM imaging on the prepared constructs. Compared to the regular scanning electron microscopy technique, cryo-SEM allows the imaging of suspended samples in their native state without the need for drying, thus avoiding specimen collapse and providing a more accurate look at the dispersed and hydrated constructs. Samples were prepared in deionized water instead of HBG buffer to minimize the interference of glucose in the sample. However, a small amount of glucose was still present in the PEI stock solution; this is observed as thin membrane-like structures upon sublimation of solvent (Figure 4).

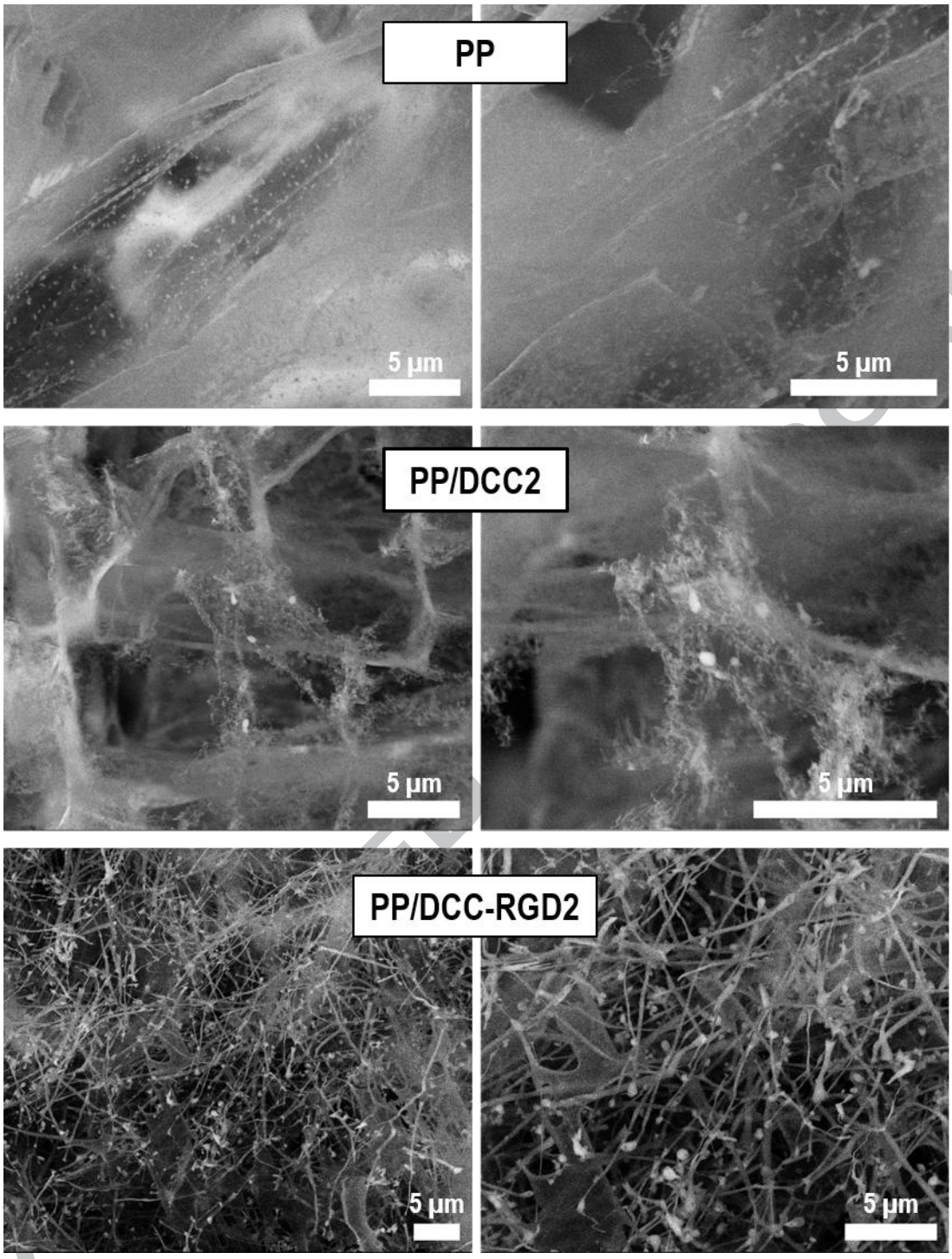

Figure 4. Cryo-SEM images of (from top to bottom): PP, DCC2, and DCC-RGD2 at lower (left column) and higher (right column) magnification

From Figure 4, we could observe that the three types of constructs had very different morphologies. PP showed the expected morphology of spherical particles with a diameter of approximately 100 nm. Similar shape and dimension have also been reported for PEI/DNA polyplexes using various techniques [31-34]. The rough dimension obtained from cryo-SEM image was also confirmed through a dynamic laser scattering measurement (Z-average=100 nm, polydispersity index (PDI)=0.24, Figure 5). PP/DCC2 showed fluffy structures similar to parallel-aligned aggregation previously reported upon addition of salt above a certain threshold [35]. We have also observed similar aggregate morphology on other chemically modified cellulose nanofibrils in the presence of physiological salt concentration (manuscript under preparation). Further, the cryo-SEM images of PP/DCC2 also showed distinct polyplexes entrapped within the aggregate structures of networked DCC (Figure 4b and Figure S2). This attachment is presumably driven by an electrostatic interaction between cationic polyplexes and anionic DCC. The images also confirm that the morphology of the polyplexes stayed roughly

spherical, indicating that pDNA stayed condensed as a polyplex with the PEI in agreement with the gel retardation assay results (Figure 3).

In contrast to those of polyplex and PP/DCC2 systems, the cryo-SEM images of PP/DCC-RGD2 showed a more defined self-assembled fibrillar structure of DCC-RGD2 with diameters ranging from 130 nm to 500 nm and lengths in the micrometer scale. These diameters are much larger than the reported diameter of elementary nanofibrils [36, 37], indicating that this chain-building assembly happened both through lateral and end-to-end association. As with PP/DCC2, spherical polyplexes were also visible that were evenly scattered and in close proximity to the surface of the fibrillar network.

We hypothesize that the presence of RGD on the crystal surface likely enhances crystal-to-crystal association through a combined effect of reduced repulsion and bridging flocculation [38]. A similar side-by-side and end-to-end association has also been reported for sulfated CNC [39], CNCs functionalized with diamines through carbodiimide coupling [40], complementary strands of DNA [15], and polyphosphoesters [41]. Typically, the tendency for end-to-end association may be caused by the

anisotropic geometry of CNCs, which may facilitate the preferential alignment of crystals along the long axis, or by the chiral properties of CNCs [42].

3.5. Dynamic Light Scattering (DLS)

To obtain a better understanding of the interactions between PP and both CNCs, we also employed DLS to estimate the size and zeta potential of the reported formulations. Due to the sedimentation of DCC-RGD-based constructs, size measurements provided inaccurate results and were therefore excluded. The zeta potential of DCC-RGD-based constructs was measured after pre-incubating the samples for sufficient sedimentation; thus, the measured electrophoretic mobility was not critically affected by gravity-induced sedimentation.

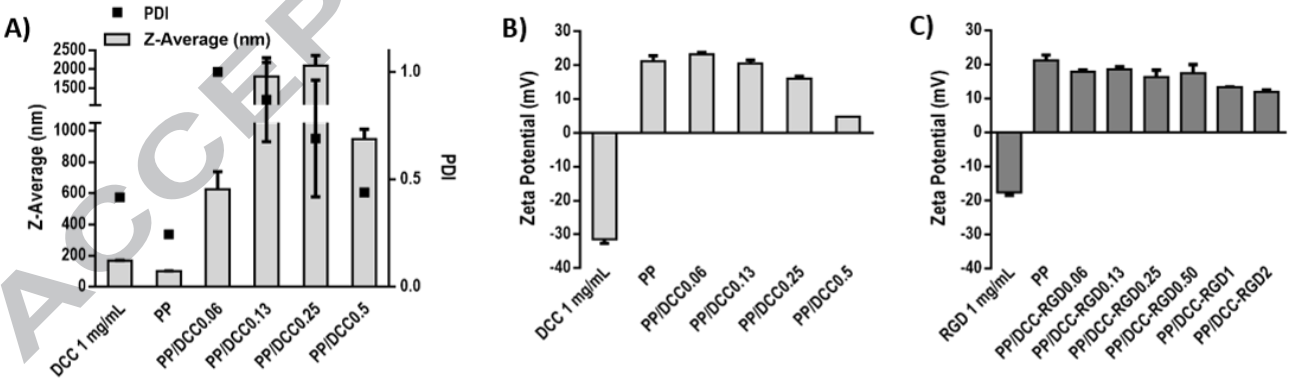

Figure 5. (A) Z-average data on DCC-based constructs. (B) Zeta-potential data on DCC-based constructs. (C) Zeta-potential data on DCC-RGD-based constructs. Measurements were also done on PP

without CNC and 1 mg/mL dispersions of pure DCC and DCC-RGD in HBG (first two bars on each graph).

As shown in Figure 5, PP without the addition of CNC showed a Z-average of 100 nm with a relatively narrow PDI of 0.24 and a zeta potential of +21.2 ± 1.6 mV. Meanwhile, individual, elongated DCC without PP showed a Z-average of 167.3 nm (PDI = 0.42), and a zeta potential of -31.5 ± 1.2 mV. As expected, PP was positively charged due to the protonated amines on PEI, while DCC was negatively charged due to the presence of carboxylic acids. Upon functionalization with RGD, DCC-RGD showed a lower zeta potential value of -17.8 ± 0.8 mV, indicating reduced colloidal stability, which potentially served also as the driving force for the fibrillar self-assembly.

The addition of CNC into PP solution caused the overall zeta potential to decrease in a concentration-dependent manner. A higher concentration of either DCC or DCC-RGD caused a greater reduction in zeta potential. This result in combination with the cryo-SEM images signifies the role of electrostatic interactions in the formation of constructs between PP and CNCs. On DCC-based constructs, this interaction induced the formation of large aggregates with a very high

PDI. Since the result of gel retardation assay indicated that PP remained intact (Figure 3), aggregates likely occurred without the disruption of the spherical shape of PP, as was also indicated by cryo-SEM images (Figure 4).

3.6. Transfection of NIH3T3 in vitro

We initially investigated DCC as a potential coating to reduce the cytotoxicity of PP using the fibroblast NIH3T3 cell line. We predicted that addition of DCC on polyplex formulation may reduce cytotoxicity by reducing the highly positive charges of the polyplexes. A potential drawback of this approach, however, is that the less–positive charges of the polyplex may decrease cellular uptake through the reduced electrostatic interactions between the polyplexes and the cell membrane. Such an effect was reported by Mahmoud et al., who found that negatively charged fluorescein isothiocyanate-functionalized CNC was less internalized by cells than positively charged rhodamine B isothiocyanate-functionalized CNC [9]. Thus, to circumvent this effect, we investigated two incubation durations (i.e., the duration during which the constructs were in contact with the cells), 4 h and 48 h.

As a control, we also tested mixing CNC with pDNA prior to the addition of PEI. Such construct was found to significantly diminish transfection (Figure S3), indicating that presence of CNC prior to PP formation interfered negatively with the complexation between PEI and pDNA.

PP without additional DCC provided a high transfection efficiency of approximately 40% at 4 h incubation duration (Figure 6). However, the cell viability was slightly less than 50%. When the incubation duration was increased to 48 h, most cells were no longer metabolically active with lower and highly deviating transfection efficiency. This result is consistent with various reports on the cytotoxicity of PEI-based transfection agents [23, 24].

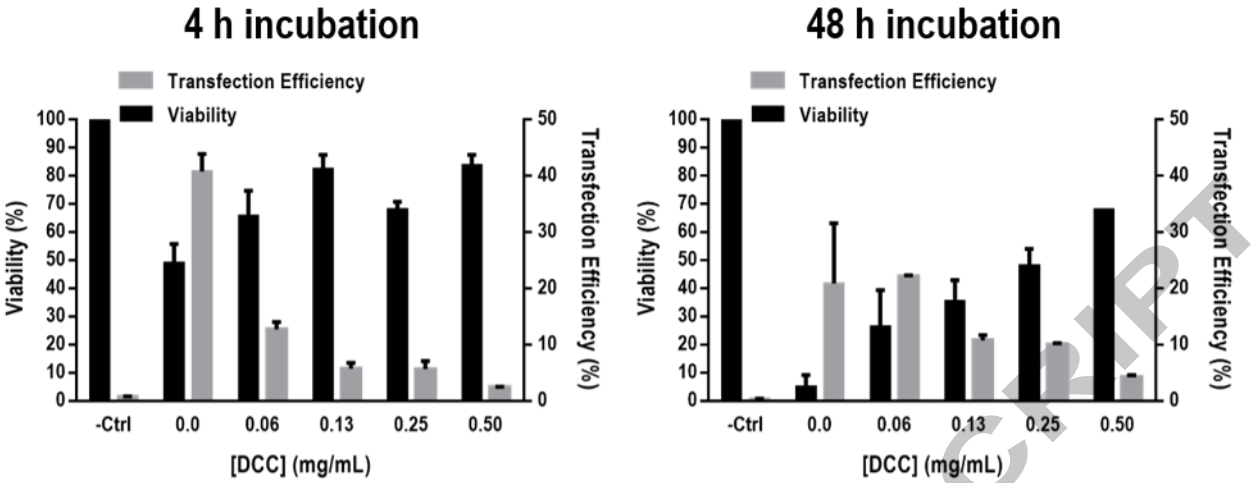

Figure 6. Viability and transfection efficiency of NIH3T3 cells treated with PP with various DCC concentrations for 4 h (left) and 48 h (right).

In general, a higher DCC concentration led to greater cell viability, both at 4 h and 48 h of incubation. However, the increase in cell viability was also accompanied by a significant decrease in transfection efficiency. For 4 h incubation duration, the addition of even the lowest concentration of DCC reduced the transfection efficiency to 13%, although the viability was slightly increased to 66%. Overall, the number of viable transfected cells can be estimated to be lower for PP/DCC0.06 than PP without DCC.

In the presence of DCC, 48 h of incubation almost doubled the transfection efficiency compared to that of 4 h incubation, but at a lower viability. However, the optimal transfection efficiency achieved by PP without DCC at 4 h incubation (i.e., 40%) was still not achievable in the

presence of DCC. This phenomenon likely indicates that DCC simply postponed the onset of cytotoxicity at the expense of transfection efficiency.

These results show that an optimal and improved formulation of PP through the addition of DCC is difficult to achieve. Therefore, we proceeded to functionalize DCC with RGD tripeptide to improve cellular uptake, transfection efficiency and to provide cell targeting.

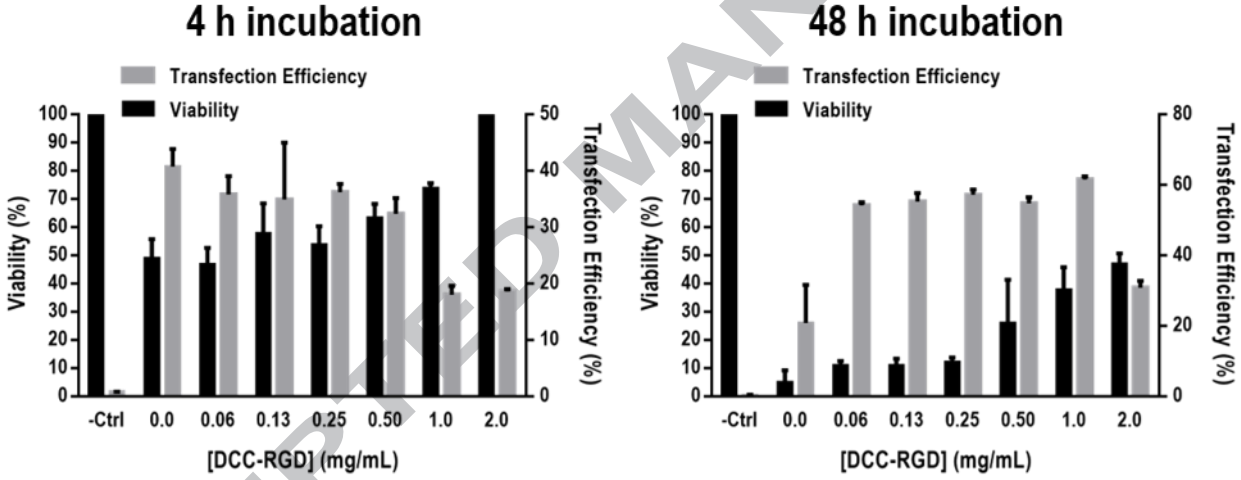

Figure 7. Viability and transfection efficiency of NIH3T3 cells treated with PP with various DCC-RGD concentrations for 4 h (left) and 48 h (right).

As shown in Figure 7, polyplex formulations containing DCC-RGD provided improved viability (as was also observed for DCC, Figure 6) but without a significant loss in transfection efficiency. At 4 h incubation duration, PP/DCC-RGD0.5 provided a viability of almost

70% while maintaining a transfection efficiency of approximately 32%. Further increasing the DCC-RGD concentration led to further improved viability but decreased the transfection efficiency to 20%.

Interestingly, an increase in incubation duration to 48 h increased transfection efficiency to over 50%, which is higher than the optimal transfection efficiency achieved for PP without CNC at 4 h incubation duration (i.e., 40%). Although viability was not significantly improved at lower concentrations of RGD at 48 h incubation duration, PP/DCC-RGD1 provided significantly higher viability with a transfection efficiency of up to 60% (Figure 7, right). The less pronounced improvement in viability compared to DCC-based constructs (Figure 6) might be due to the higher level of transfection efficiency that interfered with the normal metabolic activity of cells. The highest viability at 48 h of incubation was observed at the highest DCC-RGD concentration at only 50% viability, and with a significantly reduced transfection efficiency. This result indicates that the more optimal incubation duration for both types of CNC was 4 h instead of 48 h, signifying the importance of removing excess reagents to prevent cytotoxicity. The

exact optimal incubation duration, however, could fall somewhere between 4 and 48 h, where the highest transfection efficiency is potentially achieved directly prior to the removal of excess reagents.

The significant difference in the performance of DCC- and DCC-RGD-based constructs is likely attributed to several factors. The first factor is the reduced zeta potential of DCC-RGD compared to DCC, which may decrease electrostatic repulsion with cell membrane, thereby facilitating better cell attachment. The second factor is the presence of the RGD motif on the surface of DCC-RGD, which is known to enhance cellular adhesion on nanocellulose [43], potentially improving cellular uptake. The third factor is the distinct shape and size of the DCC-RGD-based construct with respect to those of DCC-based constructs. The elongated and networked morphology likely increases the sedimentation rate, thus bringing a higher concentration of PP closer to the cell membrane.

We propose that the enhanced gravitational effect due to the larger size of DCC-RGD plays a significant role in its efficacy. When this is combined with electrostatic interactions with PP and enhanced cellular

recognition due to the RGD motif, it creates an effective environment for the efficient uptake of a high PP density, while at the same time providing sufficient shielding to prevent excessive cytotoxicity. This view is in agreement with the recent finding highlighting the importance of gravitation on PEI-mediated transfection [44].

3.7. Transfection of MDCK-WT and MDCK-αVKO in vitro

To further understand the potential of the as-prepared constructs, we attempted transfection experiments using the epithelial MDCK cell line which is known to be difficult to transfect. Our initial attempt also included PP/DCC0.5, which, as with NIH3T3 cells, did not result in any significant transfection (Figure S4). Therefore, we focused our efforts on PP/DCC-RGD constructs, optimizing the DCC-RGD content. To assess the specificity of the RGD-based approach, we compared the transfections efficiencies in wild type (WT) and αV-integrin knockout (αVKO) cell lines. αV-integrins are the main RGD-binding receptors in MDCK cells [45]. Therefore, MDCK-αVKO cells have significantly fewer specific recognition sites for DCC-RGD that should reduce PP uptake and eventually also the transfection efficiency. The transfection

procedure was kept consistent with that used for NIH3T3 cells, but the incubation duration was limited to only 4 h, in view of the trend observed from the experiments with NIH3T3 cells (Section 3.6).

Figure 8 shows that without DCC-RGD, both cells experienced high cytotoxicity and very low transfection efficiency, in line with other reports on MDCK cells using similar polymeric vector [46]. Upon the addition of DCC-RGD, however, both the transfection efficiency and viability were significantly improved. Viability improved as a function of DCC-RGD concentration, as was observed with NIH3T3 cells, with a minimum viability of 70% for both MDCK-WT and MDCK-αVKO. However, unlike with the NIH3T3 cells treated with the same 4 h of incubation, the transfection efficiency did not decrease with higher concentration of DCC-RGD, but instead increased steadily. Remarkably, a transfection efficiency as high as 36% was achievable for PP/DCC-RGD2 with MDCK-WT. The trend of an increasing transfection efficiency with an increasing concentration of DCC-RGD was also observed for MDCK-αVKO, although in general the transfection efficiency was much lower than that of MDCK-WT. We note that

although αV-integrins are the most abundant RGD-binding receptors in MDCK cells, they also express low levels of other RGD-binding integrins, such as α5β1 [45]. The additional modes of binding can promote PP uptake, leading to the observed concentration-dependent increase in transfection efficiency also with MDCK-αVKO cells. Regardless, the significant difference in transfection efficiency of MDCK-WT and MDCK-αVKO cells indicates that the DCC-RGD2 may facilitate preferential uptake for cells expressing higher number of RGD-receptors.

We note that further studies are needed to elucidate the specific biological mechanism for the recognition in relation to the characteristics of the constructs as well as the cell types. It is particularly interesting to note that an increasing DCC-RGD concentration improved the transfection efficiencies for MDCK-WT but not for NIH-3T3 cells, likely indicating different cellular recognition mechanisms.

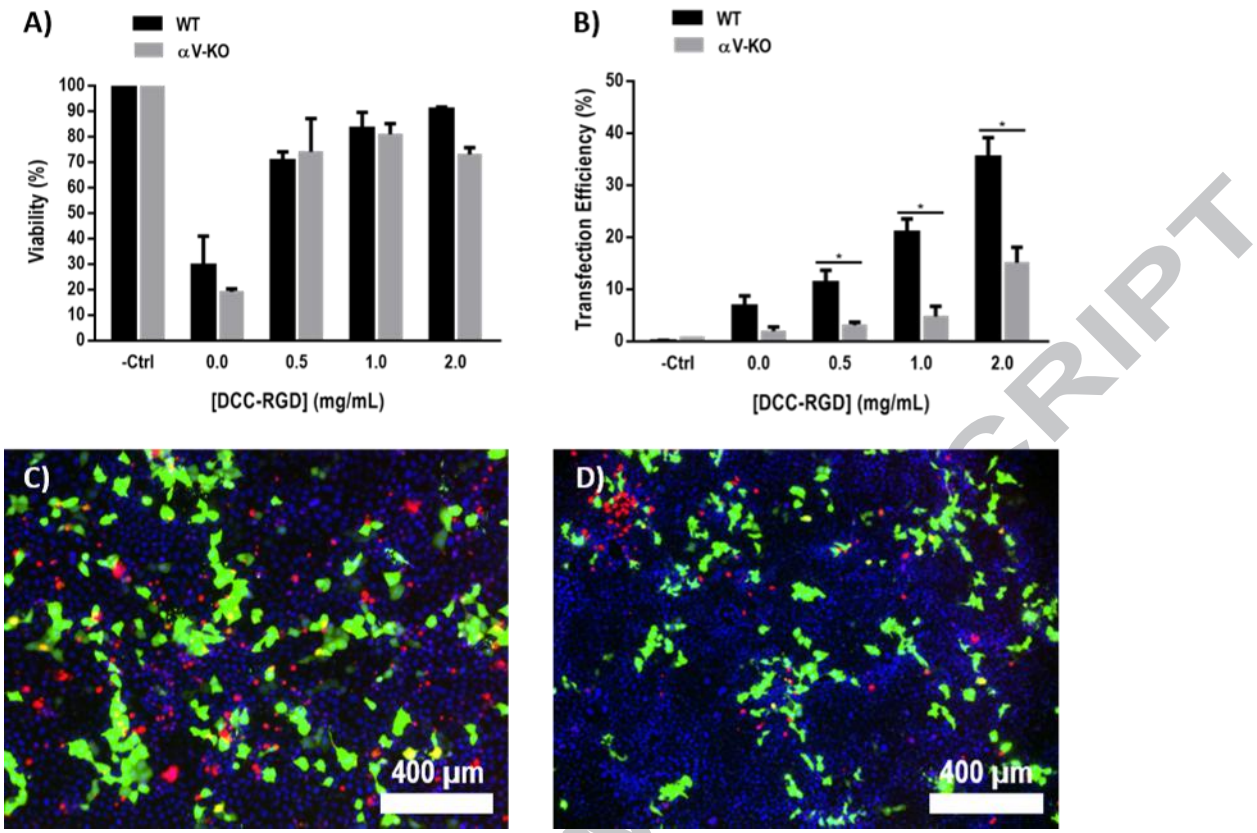

Figure 8. Viability (A) and transfection efficiency (B) of MDCK-WT and MDCK-αVKO cells treated with PP with various DCC-RGD concentrations for 4 h (Significantly different ($p < 0.05$)), as well as the overlay fluorescence image of MDCK-WT (C) and MDCK-αVKO (D) two days after transfection with PP/DCC-RGD2. Live cells were stained for their nuclei with Hoechst 33342 (blue) and dead cells were stained with propidium iodide (red), while green represents transfected GFP-positive cells.*

To obtain more insight into the role of gravitational effect on the observed transfection efficiency of MDCK-WT cells, we sonicated DCC-RGD2 prior to adding it into the PP solution and studied its efficacy in comparison to non-sonicated DCC-RGD2. Sonication disintegrated the self-assembled nanofibrillar structure, and the resulting

solution was visually transparent without noticeable sedimentation, similar to the DCC solution.

As observed in Figure 9, while there was no significant difference in the cell viability, the transfection efficiency was significantly diminished when sonicated DCC-RGD2 was used. This result indicates that the formation of self-assembled nanofibrils of DCC-RGD plays an important role in inducing efficient transfection. This is likely due to the gravitational effect, as previously discussed. Additionally, the maintained viability may also indicate the prominent interaction between PP and DCC-RGD. It can be predicted that as the sonicated DCC-RGD stayed suspended in the culture medium, excess PP was also kept in suspension due to the electrostatic interaction. On the other hand, the non-sonicated DCC-RGD likely acted like a net that sinks onto the cell monolayer, bringing the electrostatically attached PP close to the cells, thus improving both transfection efficiency and viability. These results also confirm the recent report on the importance of the gravitational force in *in vitro* transfection experiments [44].

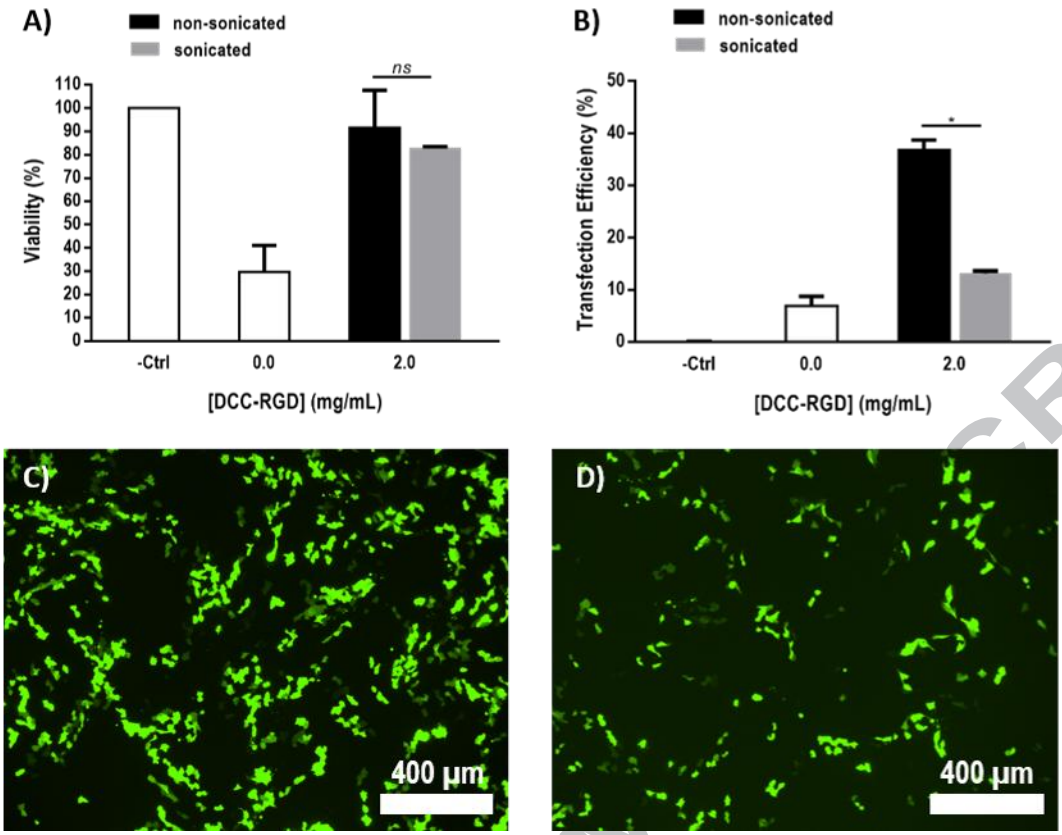

*Figure 9. Viability (A) and transfection efficiency (B) of MDCK-WT cells two days after transfection with PP/DCC-RGD2 for 4 h. The DCC-RGD2 was either sonicated or not sonicated prior to the addition into the polyplex solution. * Significantly different ($p < 0.05$), ns = not significant ($p > 0.05$). (C and D) GFP fluorescence images of MDCK-WT cells two days after transfection with PP/DCC-RGD2 prepared with non-sonicated (C) and sonicated (D) DCC-RGD2 dispersion.*

4. Conclusion

The development of nanoparticle-based drug and gene delivery system has been at the forefront of medical technology. Many nanoparticle-based systems have been found to show tremendous potential in vitro, or for certain applications, but their translation into new applications is often complicated, requiring changes in chemical composition that

sometimes alter the original properties. We hypothesized that natural high-aspect-ratio nanoparticles such as the cellulose nanocrystal may be used as an addition to an existing system, in order to improve its performance or to fulfil a new role or function. The advantage of using CNCs lies in its ease of chemical modification, and its high aspect ratio that provides a chiral nematic properties that have not received wide attention particularly in the biomedical or biomaterial field.

In this report, we have shown that functionalization of RGD tripeptide on the surface of dicarboxylic acid cellulose (DCC) nanocrystals through carbodiimide coupling was possible and resulted in a self-assembly of individual nanocrystals to fibrillar networked structure. We further showed that when added as an excipient for the model PEI-based polyplex, the self-assembled DCC-RGD could maintained transfection efficiency while improving cell viability, which we proposed to be due to the presence of RGD motif, and the pronounced gravitational effect from the self-assembled fibrillar structure of DCC-RGD. We also showed that the self-assembled DCC-RGD could provide more selective delivery of polyplexes into cells expressing more RGD-receptors, a

property that would not be as pronounced without the formation of self-assembled structure.

The concept of coating an existing nanoparticle system is not new. However, most rely on natural or synthetic polymers that essentially conform to the shape of the nanoparticle without significant changes in the surface morphology [47-50]. CNCs may provide a new way of coating that not only alter surface chemistries, but also the surface topography of nanoparticles, and hence also their interaction with biological systems [25, 26]. Further understanding on the cellular mechanism of recognition and internalization of polyplexes in the presence of CNC in general, and DCC-RGD more specifically will be an important step forward to provide new understanding on better design of materials for cellular engineering.

Although the reported constructs may not be applicable for in vivo gene delivery as such, they are still applicable for *in vitro* and *ex vivo* transfection purposes, for example on patient-derived mesenchymal stem cells which are notoriously more difficult to transfect [51], or when cell-selective transfection is required. The self-assembled fibrillar

structure of DCC-RGD may also be utilized to modify of biomedical surfaces for the study of cellular recognition, surface-mediated transfections, and/or for bottom-up tissue engineering purposes.

5. Author Information

Corresponding Author
*E-mail: Henrikki.Liimatainen@oulu.fi

Notes

Declarations of interest: none.

6. Acknowledgement

The authors would like to thank Mr. Kaitao Zhang for his help with the synthesis of CNC-DCC, Mrs. Elisa Wirkkala for performing the elemental analysis, Dr. Virpi Glumoff for her help with the flow cytometry, Ville Karvonen for his help with the TEM imaging of DCC CNC, the Biocenter Finland and Prof. Dirk Grijpma for providing fluorescence microscopy and DLS facility, respectively. Sandhanakrisnan Cattavarayane and Biocenter Oulu Virus core are acknowledged for their help in the generation of viral CRISPR-KO vectors for the study. Funding: This work was supported by the Academy of Finland (NanoBioMass project 307535).

7. References

[1] R.J. Moon, A. Martini, J. Nairn, J. Simonsen, J. Youngblood, Cellulose nanomaterials review: structure, properties and nanocomposites, Chemical Society Reviews, 40 (2011) 3941-3994.
[2] M. Kaushik, A. Moores, Review: nanocelluloses as versatile supports for metal nanoparticles and their applications in catalysis, Green Chemistry, 18 (2016) 622-637.
[3] A. Liu, A. Walther, O. Ikkala, L. Belova, L.A. Berglund, Clay Nanopaper with Tough Cellulose Nanofiber Matrix for Fire Retardancy and Gas Barrier Functions, Biomacromolecules, 12 (2011) 633-641.
[4] J.A. Sirviö, A. Kolehmainen, M. Visanko, H. Liimatainen, J. Niinimäki, O.E.O. Hormi, Strong, Self-Standing Oxygen Barrier Films from Nanocelluloses Modified with Regioselective Oxidative Treatments, ACS Applied Materials & Interfaces, 6 (2014) 14384-14390.
[5] N. Drogat, R. Granet, V. Sol, A. Memmi, N. Saad, C. Klein Koerkamp, P. Bressollier, P. Krausz, Antimicrobial silver nanoparticles generated on cellulose nanocrystals, Journal of Nanoparticle Research, 13 (2011) 1557-1562.
[6] K.A. Mahmoud, K.B. Male, S. Hrapovic, J.H.T. Luong, Cellulose Nanocrystal/Gold Nanoparticle Composite as a Matrix for Enzyme Immobilization, ACS Applied Materials & Interfaces, 1 (2009) 1383-1386.
[7] S. Dong, M. Roman, Fluorescently Labeled Cellulose Nanocrystals for Bioimaging Applications, Journal of the American Chemical Society, 129 (2007) 13810-13811.
[8] J.-L. Huang, C.-J. Li, D.G. Gray, Cellulose Nanocrystals Incorporating Fluorescent Methylcoumarin Groups, ACS Sustainable Chemistry & Engineering, 1 (2013) 1160-1164.
[9] K.A. Mahmoud, J.A. Mena, K.B. Male, S. Hrapovic, A. Kamen, J.H.T. Luong, Effect of surface charge on the cellular uptake and cytotoxicity of fluorescent labeled cellulose nanocrystals, ACS Applied Materials and Interfaces, 2 (2010) 2924--2932.

[10] S. Dong, H.J. Cho, Y.W. Lee, M. Roman, Synthesis and cellular uptake of folic acid-conjugated cellulose nanocrystals for cancer targeting, Biomacromolecules, 15 (2014) 1560--1567.
[11] J.V. Edwards, N. Prevost, K. Sethumadhavan, A. Ullah, B. Condon, Peptide conjugated cellulose nanocrystals with sensitive human neutrophil elastase sensor activity, Cellulose, 20 (2013) 1223-1235.
[12] H. Rosilo, J.R. McKee, E. Kontturi, T. Koho, V.P. Hytönen, O. Ikkala, M.A. Kostiainen, Cationic polymer brush-modified cellulose nanocrystals for high-affinity virus binding, Nanoscale, 6 (2014) 11871-11881.
[13] H. Hu, W. Yuan, F.S. Liu, G. Cheng, F.J. Xu, J. Ma, Redox-responsive polycation-functionalized cotton cellulose nanocrystals for effective cancer treatment, ACS Appl Mater Interfaces, 7 (2015) 8942-8951.
[14] G.M.A. Ndong Ntoutoume, V. Grassot, F. Brégier, J. Chabanais, J.-M. Petit, R. Granet, V. Sol, PEI-cellulose nanocrystal hybrids as efficient siRNA delivery agents—Synthesis, physicochemical characterization and in vitro evaluation, Carbohydrate Polymers, 164 (2017) 258-267.
[15] A.P. Mangalam, J. Simonsen, A.S. Benight, Cellulose/DNA Hybrid Nanomaterials, Biomacromolecules, 10 (2009) 497-504.
[16] H. Yang, T.G.M. van de Ven, A Bottom-up Route to a Chemically End-to-End Assembly of Nanocellulose Fibers, Biomacromolecules, 17 (2016) 2240-2247.
[17] M.A. Karaaslan, G. Gao, J.F. Kadla, Nanocrystalline cellulose/β-casein conjugated nanoparticles prepared by click chemistry, Cellulose, 20 (2013) 2655-2665.
[18] I. Filpponen, D.S. Argyropoulos, Regular Linking of Cellulose Nanocrystals via Click Chemistry: Synthesis and Formation of Cellulose Nanoplatelet Gels, Biomacromolecules, 11 (2010) 1060-1066.
[19] F. Wang, Y. Li, Y. Shen, A. Wang, S. Wang, T. Xie, The Functions and Applications of RGD in Tumor Therapy and Tissue Engineering, International Journal of Molecular Sciences, 14 (2013) 13447-13462.

[20] J. Park, K. Singha, S. Son, J. Kim, R. Namgung, C.O. Yun, W.J. Kim, A review of RGD-functionalized nonviral gene delivery vectors for cancer therapy, Cancer Gene Therapy, 19 (2012) 741.
[21] U. Hersel, C. Dahmen, H. Kessler, RGD modified polymers: biomaterials for stimulated cell adhesion and beyond, Biomaterials, 24 (2003) 4385-4415.
[22] S.L. Bellis, Advantages of RGD peptides for directing cell association with biomaterials, Biomaterials, 32 (2011) 4205-4210.
[23] S.M. Moghimi, P. Symonds, J.C. Murray, A.C. Hunter, G. Debska, A. Szewczyk, A two-stage poly(ethylenimine)-mediated cytotoxicity: implications for gene transfer/therapy, Molecular Therapy, 11 (2005) 990-995.
[24] V. Kafil, Y. Omidi, Cytotoxic Impacts of Linear and Branched Polyethylenimine Nanostructures in A431 Cells, BioImpacts : BI, 1 (2011) 23-30.
[25] S. Dasgupta, T. Auth, G. Gompper, Shape and Orientation Matter for the Cellular Uptake of Nonspherical Particles, Nano Letters, 14 (2014) 687-693.
[26] N.P. Truong, M.R. Whittaker, C.W. Mak, T.P. Davis, The importance of nanoparticle shape in cancer drug delivery, Expert Opin Drug Deliv, 12 (2015) 129-142.
[27] T. Selkälä, J.A. Sirviö, G.S. Lorite, H. Liimatainen, Anionically Stabilized Cellulose Nanofibrils through Succinylation Pretreatment in Urea-Lithium Chloride Deep Eutectic Solvent, ChemSusChem, 9 (2016) 3074--3083.
[28] O. Shalem, N.E. Sanjana, E. Hartenian, X. Shi, D.A. Scott, T. Mikkelson, D. Heckl, B.L. Ebert, D.E. Root, J.G. Doench, F. Zhang, Genome-scale CRISPR-Cas9 knockout screening in human cells, Science, 343 (2014) 84-87.
[29] S. Cattavarayane, R. Palovuori, J. Tanjore Ramanathan, A. Manninen, α6β1- and αV-integrins are required for long-term self-renewal of murine embryonic stem cells in the absence of LIF, BMC Cell Biology, 16 (2015) 3.

[30] J. Schindelin, I. Arganda-Carreras, E. Frise, V. Kaynig, M. Longair, T. Pietzsch, S. Preibisch, C. Rueden, S. Saalfeld, B. Schmid, J.-Y. Tinevez, D.J. White, V. Hartenstein, K. Eliceiri, P. Tomancak, A. Cardona, Fiji: an open-source platform for biological-image analysis, Nature Methods, 9 (2012) 676.
[31] Q. Peng, Z. Zhong, R. Zhuo, Disulfide Cross-Linked Polyethylenimines (PEI) Prepared via Thiolation of Low Molecular Weight PEI as Highly Efficient Gene Vectors, Bioconjugate Chemistry, 19 (2008) 499-506.
[32] N. Farkas, P. V. Scaria, M. C. Woodle, J. A. Dagata, Physical-chemical measurement method development for self-assembled, core-shell nanoparticles, 2019.
[33] A.V. Ulasov, Y.V. Khramtsov, G.A. Trusov, A.A. Rosenkranz, E.D. Sverdlov, A.S. Sobolev, Properties of PEI-based polyplex nanoparticles that correlate with their transfection efficacy, Mol Ther, 19 (2011) 103-112.
[34] H. Zhou, X. Ma, Y. Liu, L. Dong, Y. Luo, G. Zhu, X. Qian, J. Chen, L. Lu, J. Wang, X. Gao, Linear polyethylenimine-plasmid DNA nanoparticles are ototoxic to the cultured sensory epithelium of neonatal mice, Molecular medicine reports, 11 (2015) 4381-4388.
[35] C. Honorato-Rios, C. Lehr, C. Schütz, R. Sanctuary, M.A. Osipov, J. Baller, J.P.F. Lagerwall, Fractionation of cellulose nanocrystals: enhancing liquid crystal ordering without promoting gelation, NPG Asia Materials, 10 (2018) 455-465.
[36] D. Klemm, F. Kramer, S. Moritz, T. Lindström, M. Ankerfors, D. Gray, A. Dorris, Nanocelluloses: A New Family of Nature-Based Materials, Angewandte Chemie International Edition, 50 (2011) 5438-5466.
[37] S.D. Hujaya, G.S. Lorite, S.J. Vainio, H. Liimatainen, Polyion complex hydrogels from chemically modified cellulose nanofibrils: Structure-function relationship and potential for controlled and pH-responsive release of doxorubicin, Acta Biomaterialia, 75 (2018) 346-357.

[38] X. Gong, Z. Wang, T. Ngai, Direct measurements of particle–surface interactions in aqueous solutions with total internal reflection microscopy, Chemical Communications, 50 (2014) 6556-6570.
[39] F. Cherhal, B. Cathala, I. Capron, Surface charge density variation to promote structural orientation of cellulose nanocrystals, in: Nordic Pulp & Paper Research Journal, 2015, pp. 126.
[40] U.D. Hemraz, Y. Boluk, R. Sunasee, Amine-decorated nanocrystalline cellulose surfaces: synthesis, characterization, and surface properties, Canadian Journal of Chemistry, 91 (2013) 974-981.
[41] H. Wang, J. He, M. Zhang, K.C. Tam, P. Ni, A new pathway towards polymer modified cellulose nanocrystals via a “grafting onto” process for drug delivery, Polymer Chemistry, 6 (2015) 4206-4209.
[42] I. Usov, G. Nyström, J. Adamcik, S. Handschin, C. Schütz, A. Fall, L. Bergström, R. Mezzenga, Understanding nanocellulose chirality and structure–properties relationship at the single fibril level, Nature Communications, 6 (2015) 7564.
[43] A. Bodin, L. Ahrenstedt, H. Fink, H. Brumer, B. Risberg, P. Gatenholm, Modification of Nanocellulose with a Xyloglucan–RGD Conjugate Enhances Adhesion and Proliferation of Endothelial Cells: Implications for Tissue Engineering, Biomacromolecules, 8 (2007) 3697-3704.
[44] D. Pezzoli, E. Giupponi, D. Mantovani, G. Candiani, Size matters for in vitro gene delivery: investigating the relationships among complexation protocol, transfection medium, size and sedimentation, Scientific Reports, 7 (2017) 44134.
[45] T.P. Teräväinen, S.M. Myllymäki, J. Friedrichs, N. Strohmeyer, J.V. Moyano, C. Wu, K.S. Matlin, D.J. Muller, A. Manninen, αV-Integrins Are Required for Mechanotransduction in MDCK Epithelial Cells, PLOS ONE, 8 (2013) e71485.
[46] C. Wang, E. de Jong, K.A. Sjollema, I.S. Zuhorn, Entry of PIP3-containing polyplexes into MDCK epithelial cells by local apical-basal polarity reversal, in: Scientific reports, 2016, pp. 21436.

[47] S.W. Choi, W.S. Kim, J.H. Kim, Surface Modification of Functional Nanoparticles for Controlled Drug Delivery, Journal of Dispersion Science and Technology, 24 (2003) 475-487.
[48] H. Hyun, J. Park, K. Willis, J.E. Park, L.T. Lyle, W. Lee, Y. Yeo, Surface modification of polymer nanoparticles with native albumin for enhancing drug delivery to solid tumors, Biomaterials, 180 (2018) 206-224.
[49] L. Pang, Y. Pei, G. Uzunalli, H. Hyun, L.T. Lyle, Y. Yeo, Surface Modification of Polymeric Nanoparticles with M2pep Peptide for Drug Delivery to Tumor-Associated Macrophages, Pharmaceutical Research, 36 (2019) 65.
[50] M.M. Badran, M.M. Mady, M.M. Ghannam, F. Shakeel, Preparation and characterization of polymeric nanoparticles surface modified with chitosan for target treatment of colorectal cancer, International Journal of Biological Macromolecules, 95 (2017) 643-649.
[51] N.S.S.A. Halim, K.S. Fakiruddin, S.A. Ali, B.H. Yahaya, A Comparative Study of Non-Viral Gene Delivery Techniques to Human Adipose-Derived Mesenchymal Stem Cell, International Journal of Molecular Sciences, 15 (2014) 15044-15060.

Graphical abstract